Atmospheric Processes Modulating Noise in Fairfield Nodal 5 Hz Geophones

by Christopher W. Johnson, Frank Vernon, Nori Nakata, and Yehuda Ben-Zion

ABSTRACT

Atmospheric processes are documented to modulate seismic noise in Fairfield Nodal three-component geophones. Spectral analysis has shown high-amplitude signals between 40 and 50 Hz in all waveforms inspected. The changes in spectral amplitudes and frequency are found to be modified by daily variations in wind velocity and temperature, which are temporally correlated for much of the study. The wind velocity is shown to affect a wide spectral band with peak amplitudes that depend on the distance from *in situ* structures coupling wind energy into the shallow crust. The wind velocity increases the spectral amplitudes, most noticeably in the 40–50 Hz band; it produces a 15 Hz frequency modulation in the conditions of highest wind, with resonance frequencies up to 150 Hz. These signals likely reflect a superposition of multiple local and regional sources producing wind-generated ground motions and nonlinear wave propagation in the shallow subsurface. During periods of temperatures below 0°C, a similar frequency modulation is observed, but the amplitudes are not as pronounced without the elevated wind velocity. A possible source of the continuous noise signal and the temperature-dependent frequency modulation is the spike mount that is attached to the nodal housing. The noise signals modulated by the wind and temperature variations require installation procedures in order to mitigate the effects of the contaminating noise on the geophysical processes of interest.

INTRODUCTION

Fully autonomous seismic geophones, developed primarily for the petroleum industry, are increasingly being deployed by academic and research institutions for experiments that utilize 10s–1000s of sensors to address multiple geophysical questions. The compact sensors are providing high-quality data for experiments focused on subsurface imaging (Lin *et al.*, 2013; Schmandt and Clayton, 2013; Ben-Zion *et al.*, 2015; Brenguier *et al.*, 2015; Nakata *et al.*, 2015; Hillers *et al.*, 2016; Inbal *et al.*, 2016; Ward and Lin, 2017; Wu *et al.*, 2017; Mordret *et al.*, 2018), microseismic event detection (Hansen and Schmandt, 2015; Inbal *et al.*, 2015; Gradon *et al.*, 2017; Meng and Ben-Zion, 2018b), and the exploration of nontectonic signals in continuous waveforms (Johnson, Meng, *et al.*, 2018; Meng and Ben-Zion, 2018a). As the usage of these data expands and the variety of experimental design diversifies, the need to fully describe and quantify the limitations, resolution, and variability of the instruments is becoming increasingly important (Brenguier *et al.*, 2015; Farrell *et al.*, 2018; Ringler *et al.*, 2018).

The focus here is on describing spectral characteristics of the continuous waveforms from Fairfield Nodal ZLand 3C 5Hz seismic sensors, referred to as nodes, in order to examine how atmospheric processes modify the instrumental noise. The nodes are cable free with onboard Global Positioning System timing for a compact (11.7 × 16.3 cm), lightweight (2.8 kg), and easy-to-install (spike mount) all-in-one three-component geophone and data logger. Each node contains a rechargeable lithium ion battery and has 32 GB storage, with the capacity to record continuous ground motion for ~35 days at 500 samples per second. In this study, we present results with respect to the wind velocity and ambient temperature. We also show the modulation of instrumental noise, due to surface objects shaking in the wind and diurnal temperature fluctuations.

Previous efforts aimed at investigating these specific Fairfield Nodal ZLand 3C 5Hz instruments have described a persistent noise at frequencies between 10 to 100 Hz, with the largest amplitude between 20 and 40 Hz; it is postulated that this is modulated by ambient temperature changes and the degree of coupling to the ground (Farrell *et al.*, 2018). The authors have analyzed data from three different deployments and shown a high-amplitude signal around 30 Hz that modulates to higher frequencies during colder temperatures. The signal exhibits unpredictable behavior even when multiple nodes are located in close proximity, as well as a 75% amplitude increase during periods of warmer temperatures (see figs. 2 and 8 in Farrell *et al.*, 2018). Using a meteorological station that was located 2.4 km from one deployment, they found wind-generated noise spanning a broad frequency range (between 20 and 200 Hz), but they do not observe a correlation with the regional wind velocity, peak spectral amplitude, or frequency (see fig. 9 in Farrell *et al.*, 2018). The amplitude of the persistent noise is found to decrease when burying the nodes, suggesting that increased coupling is the likely cause. This is because the thermal insulation from burying 10 cm is minimal. They tested the effect of increased coupling by placing an 11 kg

doi: 10.1785/0220180383

Downloaded from https://pubs.geoscienceworld.org/ssa/srl/article-pdf/90/4/1612/4790836/srl-2018383.1.pdf
by University of Southern California user

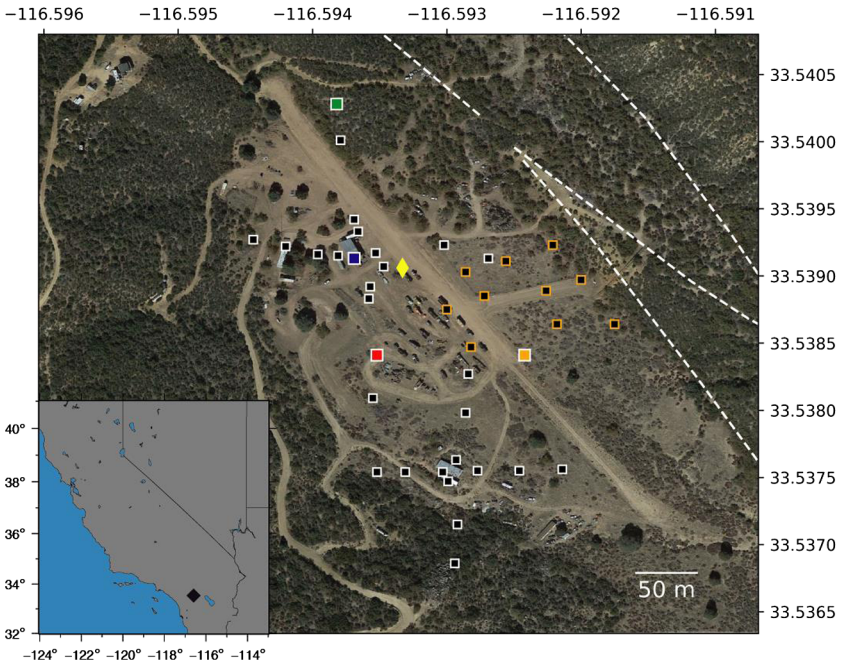

▲ **Figure 1.** Study area showing the node locations (square symbols) on Google Earth imagery with the regional inset map showing the field site with a black diamond. Black squares with white outlines are nodes used to evaluate the local structures as sources. Nodes with an orange outline are not used in the analysis. Green, blue, red, and orange squares are nodes shown for the spectral analysis in subsequent figures. The anemometer is shown as the yellow diamond. The white dashed lines represent the mapped fault trace. The color version of this figure is available only in the electronic edition.

weight on the node and found that the persistent noise remained but was altered and present at a different frequency. The only test performed that eliminates the 20–40 Hz persistent noise involved removing the spike mount and placing the node in an isolated seismic vault. The authors concluded that burying the nodes to increase ground coupling is the preferred deployment method, but the inconsistency in the response between different nodes suggests that additional processes are possibly responsible for the variations in the noise signal.

In this study, we deploy 40 nodes for 35 days to assess the modulation of noise recordings with respect to the changing wind velocity and temperature. The data were collected at the Sage Brush Flats site on the Clark branch of the San Jacinto fault near Anza, California, between 9 February and 17 March 2018 (Fig. 1). The study area is the same location as that of a previous dense nodal deployment (Ben-Zion *et al.*, 2015), and the property was formerly an active ranch that still contains unused buildings and machinery, an unused airstrip, some fencing, and natural vegetation (Fig. 1). The experiment was designed to target the wind-generated ground motions produced by the wind interaction with *in situ* structures and vegetation (Johnson, Meng, *et al.*, 2018). The instruments were deployed using the spike mount on the surface and not buried. The wind velocity was recorded on site as the 1 min average and maximum at a height of about 3.5 m, in order to get representative values of what the buildings and vegetation experience. The temperature data were obtained from the internal sensor in each node with a 30 min sampling rate; additional temperature data were also acquired from a local weather station (KCAMOUNT4) located 3 km north of the study area with a 15 min sampling rate. The wind and temperature data show diurnal fluctuations that increase by midday local time and subside during the evening and nighttime hours. The internal temperature sensor and regional measurements are very similar, with a difference of about 2°C between the daily extreme values for nodes located in direct sunlight. The waveform spectra are analyzed during discrete wind velocity intervals in order to evaluate the amplitude and frequency modulation as the wind and temperature change throughout the duration of the deployment.

The analysis is performed using the multitaper spectral method, with adaptive weights to obtain high-resolution spectral estimates for a time bandwidth product of 4 and 7 discrete prolate spheroidal sequences (Thomson, 1982; Prieto *et al.*, 2009). The instrument response is removed by deconvolving the transfer function from the detrended cosine-tapered waveforms. The data are cut into 60 s intervals and grouped by average wind velocity from 0 to 5 m/s, using a 1 m/s interval. The median of all spectra in each velocity interval represents the spectral estimate for each geophone as a function of the average wind velocity. The spectrograms are produced using 1 min intervals with 10% overlap.

NOISE AMPLIFICATION FROM WIND INTERACTION WITH SURFACE OBJECTS

The median spectra as a function of wind velocity show an increase in power throughout the 5–200 Hz band, with an increase of ~20 dB when the wind velocity is between 4 and 5 m/s (Fig. 2). The node used in this case is located between a covered parking structure and a housing structure next to unused machinery (red square in Fig. 1). The amplitude modulation is observed throughout the entire spectrum, suggesting that multiple local and regional surface objects are shaking in the wind and coupling energy to the ground. A peak around 40–50 Hz is present in all the spectra, similar to the high-amplitude signal reported by Farrell *et al.* (2018), and shows a systematic increase with the wind velocity.

The modulations of the spectral amplitude and peak frequency are further evaluated using the vertical channels of 16 nodes for a single day; these nodes extend in each cardinal direction from the covered parking structure over a distance of 10–130 m. An amplitude decay with distance is evident in all transects during wind velocities >1 m/s, suggesting that the covered parking structure is contributing to the noise as a

Downloaded from https://pubs.geoscienceworld.org/ssa/srl/article-pdf/90/4/1612/4790836/srl-2018383.1.pdf
by University of Southern California user

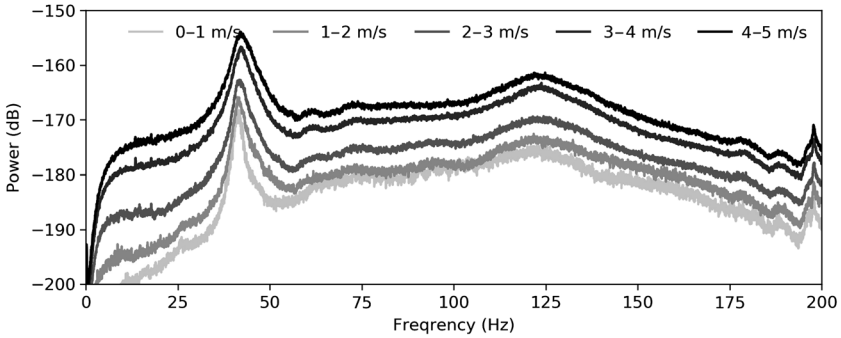

▲ **Figure 2.** Median spectra shown by average wind velocity, as indicated by the color of the curve for the red node in Figure 1 located near the unused machines between the parking structure and housing structures.

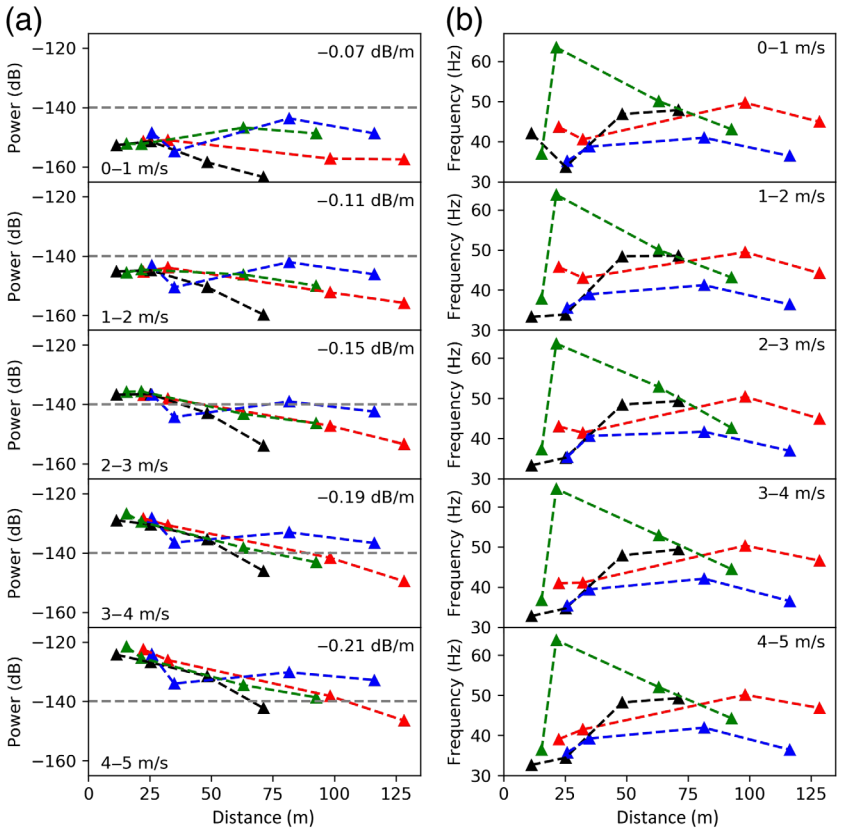

▲ **Figure 3.** (a) Spectral amplitude and (b) peak frequency are shown for the nodes around the covered parking structure, as a function of distance from the structure for 1 m/s wind velocity intervals. The transect directions are shown as red (north), green (east), blue (south), and black (west) line, with the decay in power as a function of distance shown for each panel. The color version of this figure is available only in the electronic edition.

local source (Fig. 3). When the wind velocity is between 4 and 5 m/s, a decrease of 25 dB is observed at distances of more than 130 m. The peak frequency remains nearly constant at each location during the changing wind conditions, with variations representing site-specific conditions. Within 25 m of the parking structure, the peak frequency is 35–45 Hz and shifts to >40 Hz as the distance increases in all directions. The second node on the east transect shows a peak frequency that is abnormally high at ~65 Hz, which is not observed at other sensors installed in similar conditions; this highlights the variability in the ground motions over distances of 10s of meters in the study area.

The analysis is repeated using the 12 nodes around the housing structure to the south. An amplitude decay with wind velocity is observed, but no clear indicator that the house is an isolated source is found. The building is lower in height than the covered parking structure and is situated in a position that is adjacent to the hillslope. The spectral amplitudes are lower than the nodes to the north around the parking structure. The lack of a distance dependence suggests that shaking produced by the housing structure contributes weakly to the noise and that frequency modulation is influenced by site-specific changes in the shallow subsurface on length scales of 10–30 m. The peak frequency is about 45 Hz near the housing structure in all directions except to the south, which contains large granite boulders in a hillslope. To the west, north, and east, the ground is basin fill; also, the peak frequencies systematically increase by 5–10 Hz in these directions.

SPECTRAL MODULATION WITH WIND AND TEMPERATURE

Spectrograms for the east and vertical channels are calculated starting on Julian day 50–59 and are shown with the wind and temperature data (Figs. 4–6) for three nodes located near trees (green square in Fig. 1), under the parking structure (blue square in Fig. 1), and in areas of low vegetation (orange square in Fig. 1). The temperature data from each node are shown with the regional temperature measurements in order to highlight the subtle difference in temperature between the locations. In all nodes, the horizontal amplitudes are larger than the vertical amplitudes, and both channels show an increase during elevated wind velocity (Johnson, Meng, *et al.*, 2018). The spectrograms show many interesting features associated with the daily changes in wind and temperature that vary between the nodes that are located less than 300 m apart but situated in close proximity to different surface objects and shade conditions. An increase in amplitude of more than 20–200 Hz is shown in each spectrogram during the highest wind conditions, with a peak amplitude present in the near-continuous signal between 40 and 75 Hz that correlates with the wind velocity. The frequency modulation differs

Downloaded from https://pubs.geoscienceworld.org/ssa/srl/article-pdf/90/4/1612/4790836/srl-2018383.1.pdf
by University of Southern California user

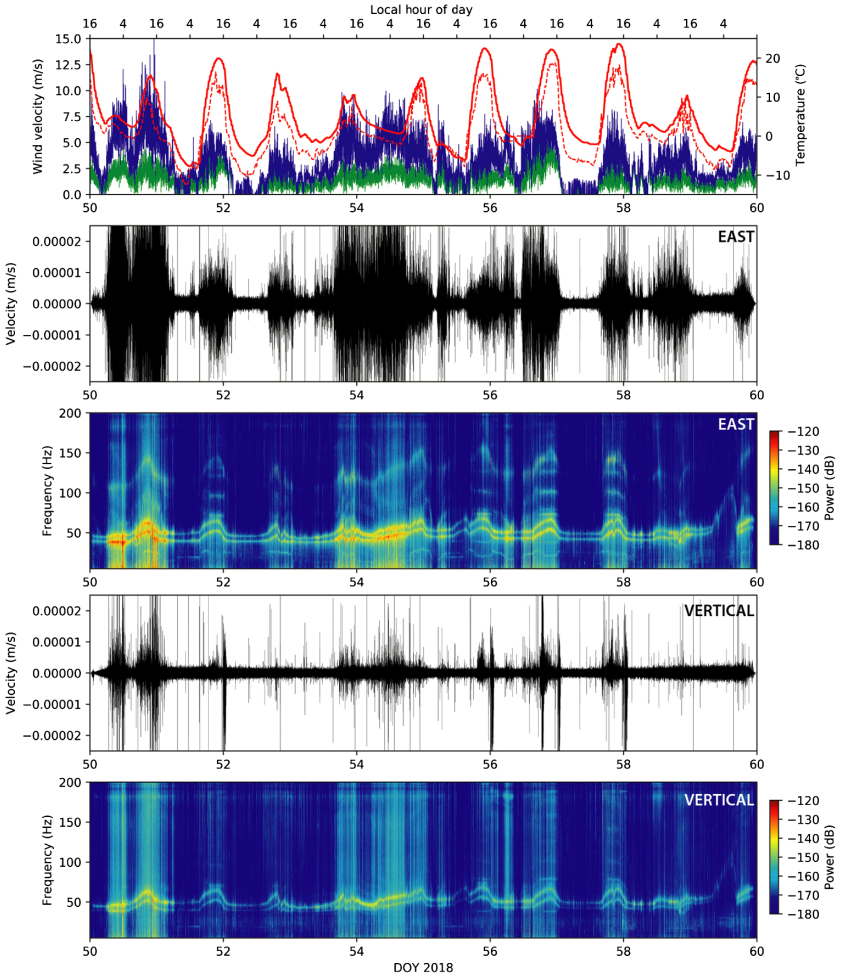

▲ **Figure 4.** The top panel shows the average (green line) and maximum (blue line) wind velocity, along with the node sensor temperature (solid red line) and regional temperature (dashed red line) for the day-of-year (DOY) shown. The additional panels show the east and vertical waveforms and spectrogram for the node located in the trees (green square in Fig. 1). The color version of this figure is available only in the electronic edition.

at each location, with an increase in peak frequency during the coldest temperatures present in the data of one of the nodes.

The node located close to the trees shows a near-continuous high-amplitude signal between 40 and 50 Hz with two distinct bands (Fig. 4). When the wind velocity is above 2 m/s, a nonlinear response is shown as the spectral amplitude within this narrowband increases, and the peak frequency increases by 15 Hz. In the horizontal channel, resonance signals are observed up to 150 Hz and exhibit the same amplitude and frequency modulations as the near-constant signal around 45 Hz. The vertical channel shows a similar spectral modulation with increased amplitude that moves to higher frequencies around 65 Hz, but the high-frequency resonance signals have much lower amplitude. The frequency modulation and presence of overtones indicate changing behavior during different wind and temperature conditions. Between day 50 and 52, there are three distinct periods of elevated wind conditions and two peaks in the temperature. When the wind and temperature increase, the spectral amplitude increases, the signal moves to higher frequencies, and resonance signals are observed in the horizontal channels. However, on day 50.5 with the elevated winds during the nighttime hours, no modulation of the frequency is observed, but the increased amplitude and resonance signals are present. Conversely, during day 54, the wind velocity remains above 2 m/s and the temperature is slowly decreasing; however, it remains above 0° C while the peak frequency is gradually increasing throughout the day over a period of many hours. The higher wind velocity produces a long-duration amplitude increase, and the high-frequency resonance signals are present.

The node located under the covered parking structure that is not exposed to direct sunlight exhibits some of the highest noise amplitudes, due to the close proximity of the structural footing that is coupling wind energy into the ground (Fig. 5). The temperature record indicates nighttime lows 2–3°C above the regional measurement, with consistent values for the daytime highs. The spectrogram shows increased power up to 200 Hz when the wind velocity is above 2 m/s, with the most pronounced increase consistently in the 40–50 Hz band. However, the record of the node does not show a shift in the peak frequency or the resonance signals that are observed for the node near the tree (Fig. 4). The peak amplitude remains in the 40–50 Hz range, with a dual band observed for the horizontal channel, similar to the node by the tree; however, only a single high-amplitude band is found in the vertical channel. On day 59, a frequency modulation is present during low-wind conditions and temperatures below 0°C that is not found during other periods of similar wind and temperature conditions, such as day 52. The lack of modulating frequency suggests that the high-amplitude ground shaking induced by the close proximity parking structure is obscuring the ability to observe other resonance frequencies.

The node located in the low-vegetation area and direct sunlight adjacent to the unused runway shows a mix of features found in the other two nodes (Fig. 6). The daytime high temperature is 0–2°C above the regional measurement, with consistent lows. The spectrogram shows an increase in amplitude from 20 to 200 Hz, correlating with the changing wind velocity. A dual band signal is observed in the horizontal channel, with a single band in the vertical. Both show an amplitude increase in this band during wind-generated ground shaking. The frequency modulation has similar characteristics to the node in the trees (Fig. 4), but the higher resonance frequencies are not observed. A noticeable difference is found on days 51.5, 55.5, and 59.9, when the nighttime temperature reduces below

Downloaded from https://pubs.geoscienceworld.org/ssa/srl/article-pdf/90/4/1612/4790836/srl-2018383.1.pdf
by University of Southern California user

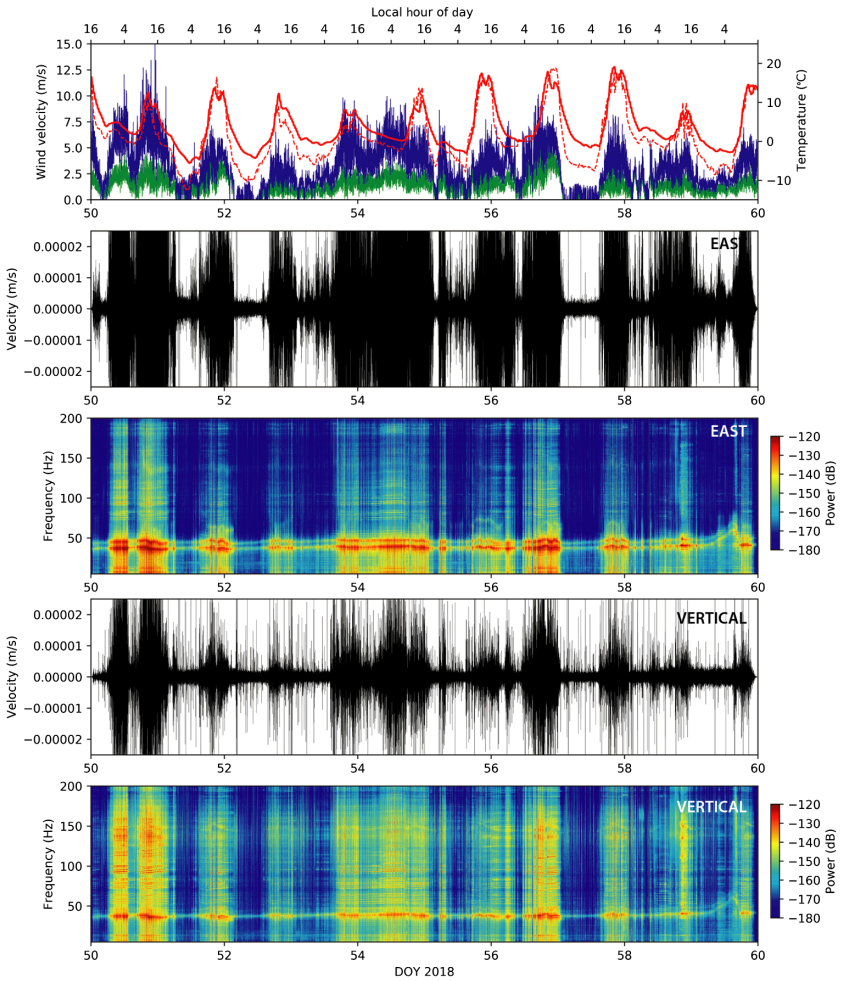

▲ **Figure 5.** Same as Figure 4 for the node located under the parking structure (blue square in Fig. 1) for the DOY shown. The color version of this figure is available only in the electronic edition.

0°C and a frequency modulation is observed up to 80–100 Hz; this is more consistent with the frequency modulation reported by Farrell *et al.* (2018) during temperatures that drop to −15°C. The signal is lower in amplitude than the wind-generated noise and increases to slightly higher frequencies than during temperatures below 0°C and elevated wind velocity.

DISCUSSION AND CONCLUSIONS

Instrumental noise in frequency bands of interest for geophysical monitoring can limit the usability of seismic data or produce inaccurate interpretations. Presented results shown in multiday spectrograms for three nodes located within 0.1 km^2 indicate nonlinear changes in spectral amplitude and frequency modulation with both increasing wind velocity and temperature fluctuations. One location exhibits resonance frequencies up to 150 Hz (Fig. 4). These signals could be produced by a superposition of multiple local sources, such as the parking structure (Fig. 2), and more distant sources from wind-driven ground shaking. Some of the frequency shifts may be produced by the highly damaged shallow propagation medium, which is shown in theory, laboratory experiments, and other seismic data to produce nonlinear wave propagation effects and changes of resonance frequencies (Johnson and Jia, 2005; Lyakhovsky *et al.*, 2009; Wu *et al.*, 2010). The exact origins of these signals are not clear but probably involve a combination of multiple sources, combined with nonlinear wave propagation effects. Resolving these and other unclear features of the data requires further investigations to mitigate problematic noise signals in a frequency band of interest.

A common feature in the data is increased power around 40–50 Hz that is modulated to higher frequencies around 65 Hz and contains different properties, depending on the sensor location in the study area. Using the same type of nodes, Farrell *et al.* (2018) described a persistent noise signal in the 20–40 Hz range that exhibited a temperature-dependent modulation of the peak frequency that increases during conditions below 0°C, but they did not observe a narrowband spectral amplitude increase related to the wind conditions. In the current study, the two nodes situated in the vegetation during wind conditions >2 m/s show an increase in the spectral amplitude and a change in peak frequency of about 15 Hz. The frequency modulation is consistently observed during increased wind conditions at these locations but is not found for the node near the parking structure (Fig. 5). Our results on a frequency modulation with decreasing temperatures (Fig. 6) concur with Farrell *et al.* (2018), but notable additional features are now described, such as the influence of the wind-generated ground motions on resonance frequencies.

The results show that the 40–50 Hz signal is modified by changing wind conditions, implying that the source of energy is naturally occurring from surface coupling and propagating through the shallow medium. This is evident by looking at the distance relationship to the noise amplitudes throughout the entire spectral range (Fig. 2), suggesting that the wind-generated ground motions are transferring high-frequency energy into the top crust. Naderyan *et al.* (2016) found a wind-dependent interaction with cabled geophones that was independent of the sensor burial depth and postulated that the observed ground displacements were produced by a nearby fence coupling to shallow layers of soil; they were not the direct interaction of the wind with the instrument. The process may stimulate natural frequencies that are associated with the design of the sensor or the attached spike mount, but the source of energy involves the wind interaction with objects in the study area. Ringler *et al.* (2018) performed a series of fidelity tests using the ZLand Fairfield 5Hz geophones in a thermally insulated environment and found a 60 Hz peak and overtones to be

Downloaded from https://pubs.geoscienceworld.org/ssa/srl/article-pdf/90/4/1612/4790836/srl-2018383.1.pdf
by University of Southern California user

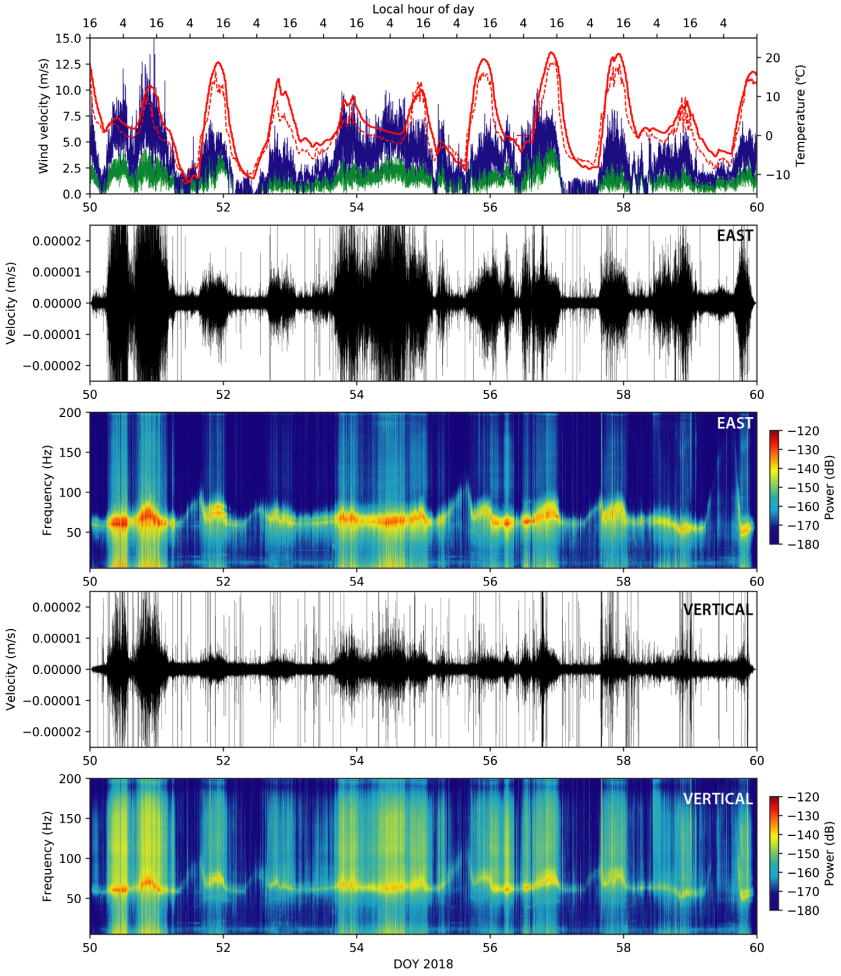

▲ **Figure 6.** Same as Figure 4 for the node located in the bushes (orange square in Fig. 1) for the DOY shown. The color version of this figure is available only in the electronic edition.

excited by noise sources inside the vault, but they did not test aspects of coupling during a field deployment. Possible evidence of this excitation is shown in the east channel in Figure 4 in which multiple resonances with peaks up to 125–150 Hz are present during periods of increased winds, possibly produced by local and more distant sources.

The increase to a higher frequency is observed when the temperature decreases below 0°C (Fig. 6), although this is only the case with lower spectral amplitudes. These observations suggest that multiple processes are contributing to the observed nonlinear response. For the temperature dependence, one possibility is that the nodes are susceptible to thermal changes of a few degrees and require additional insulation to reduce or eliminate this frequency modulation during freezing temperature conditions, especially if the signal of interest is close to these high-frequency bands. Farrell *et al.* (2018) tested burying the sensors and adding weight to provide thermal insulation and increase ground coupling, and they concluded that the spectral power increase was not coming from the ground but related to the instrument. If using the spike mount, the temperature-dependent frequency modulation could arise from improved coupling to the soil by increased rigidity; it could also be a change introduced by a subtle flexure at the adjoining baseplate to the node housing, due to moisture expansion. The clarification of such effects requires systematic testing to determine a preferred method to install the nodes with or without the spike mount.

These high-frequency signals are most directly correlated with the proximity to vegetation and *in situ* structures, suggesting that the coupling of atmosphere processes is possible through any object on the surface and should be a common feature in high-quality seismic data. The results presented only show this feature in the east component of one node, but the wind-generated ground motions excite frequencies up to 200 Hz and may obscure clear resonance signals in other nodes that experience higher noise. In areas with vegetation or other obstacles above the surface, one might expect the near-constant noise signal to be a byproduct of the obstacles coupling atmospheric energy into the shallow crust that resonates in the subsurface and instruments. The coupling of atmospheric processes to ground motion may depend on the height and other properties of the objects above the surface, suggesting that these signals would display some variability among different sites. It is possible that the process stimulates frequencies that are associated with the instrument's design, but the source of energy is naturally occurring from the interaction of the wind with objects above the surface, as well as, most likely, nonlinear wave propagation through the shallow subsurface. The presented modulation of spectral power provides evidence that the local structures and vegetation are coupling wind energy into the shallow surface, and temperature changes of a few degrees can modify the frequency content of the ZLand Fairfield nodes used in this study.

DATA AND RESOURCES

The data can be obtained from the Data Management Center of the Incorporated Research Institutions for Seismology and Broadband Seismic Data Collection (Johnson, Vernon, *et al.*, 2018). The local temperature data are available from www.wunderground.com/weatherstation/WXDailyHistory.asp?ID=KCAMOUNT4 (last accessed July 2018). Upon request, the wind data are available in .mat or .pkl binary format, and the nodal temperature sensor data presented are available in .csv format.

ACKNOWLEDGMENTS

The authors thank Editor-in-Chief Zhigang Peng and two anonymous reviewers for the constructive comments that improved the impact and readability of this article. C. W. J.

Downloaded from https://pubs.geoscienceworld.org/ssa/srl/article-pdf/90/4/1612/4790836/srl-2018383.1.pdf
by University of Southern California user

is funded by the National Science Foundation (NSF) EAR Postdoctoral Fellowship Award 1725344. The study was supported by the Southern California Earthquake Center (based on NSF Cooperative Agreement EAR-1600087 and U.S. Geological Survey [USGS] Cooperative Agreement G17AC00047) and the NSF (Grant Number EAR-1818589). The authors thank Niloufar Abolfathian, Yifang Cheng, and Haoran Meng for assisting with the deployment and Raymond Ng for removing the data from the geophones.

REFERENCES

Ben-Zion, Y., F. L. Vernon, Y. Ozakin, D. Zigone, Z. E. Ross, H. Meng, M. White, J. Reyes, D. Hollis, and M. Barklage (2015). Basic data features and results from a spatially dense seismic array on the San Jacinto fault zone, *Geophys. J. Int.* **202,** no. 1, 370–380, doi: 10.1093/gji/ggv142.

Brenguier, F., P. Kowalski, N. Ackerley, N. Nakata, P. Boué, M. Campillo, E. Larose, S. Rambaud, C. Pequegnat, T. Lecocq, *et al.* (2015). Toward 4D noise-based seismic probing of volcanoes: Perspectives from a large-N experiment on Piton de la Fournaise volcano, *Seismol. Res. Lett.* **87,** no. 1, 15–25, doi: 10.1785/0220150173.

Farrell, J., S.-M. Wu, K. M. Ward, and F.-C. Lin (2018). Persistent noise signal in the FairfieldNodal three-component 5-Hz geophones, *Seismol. Res. Lett.* **89,** no. 5, 1609–1617, doi: 10.1785/0220180073.

Gradon, C., L. Moreau, P. Roux, and Y. Ben-Zion (2017). Locating surface and shallow seismic sources using a dense array of sensors on the San Jacinto Fault, paper presented at the *American Geophysical Union Fall Meeting*, New Orleans, Louisiana, 11–15 December 2017.

Hansen, S. M., and B. Schmandt (2015). Automated detection and location of microseismicity at Mount St. Helens with a large-N geophone array, *Geophys. Res. Lett.* **42,** no. 18, 7390–7397, doi: 10.1002/2015GL064848.

Hillers, G., P. Roux, M. Campillo, and Y. Ben-Zion (2016). Focal spot imaging based on zero lag cross-correlation amplitude fields: Application to dense array data at the San Jacinto fault zone, *J. Geophys. Res.* **121,** no. 11, 8048–8067, doi: 10.1002/2016JB013014.

Inbal, A., J. P. Ampuero, and R. W. Clayton (2016). Localized seismic deformation in the upper mantle revealed by dense seismic arrays, *Science* **354,** no. 6308, 88–92, doi: 10.1126/science.aaf1370.

Inbal, A., R. W. Clayton, and J.-P. Ampuero (2015). Imaging widespread seismicity at midlower crustal depths beneath Long Beach, CA, with a dense seismic array: Evidence for a depth-dependent earthquake size distribution, *Geophys. Res. Lett.* **42,** no. 15, 6314–6323, doi: 10.1002/2015GL064942.

Johnson, C. W., H. Meng, F. Vernon, N. Nakata, and Y. Ben-Zion (2018). Characteristics of ground motion generated by interaction of wind gusts with trees, structures and other obstacles above the surface, paper presented at the *Southern California Earthquake Center Annual Meeting*, Palm Springs, California, 9–12 September 2018.

Johnson, C. W., F. Vernon, Y. Ben-Zion, and N. Nakata (2018). *Sage brush flats seismic experiment on interaction of wind with ground motion*, International Federation of Digital Seismograph Networks, doi: 10.7914/SN/7A_2018.

Johnson, P. A., and X. Jia (2005). Nonlinear dynamics, granular media and dynamic earthquake triggering, *Nature* **437,** 871–874, doi: 10.1038/nature04015.

Lin, F.-C., D. Li, R. W. Clayton, and D. Hollis (2013). High-resolution 3D shallow crustal structure in Long Beach, California: Application of ambient noise tomography on a dense seismic array, *Geophysics* **78,** no. 4, Q45–Q56, doi: 10.1190/geo2012-0453.1.

Lyakhovsky, V., Y. Hamiel, J.-P. Ampuero, and Y. Ben-Zion (2009). Nonlinear damage rheology and wave resonance in rocks, *Geophys. J. Int.* **178,** no. 2, 910–920, doi: 10.1111/j.1365-246X.2009.04205.x.

Meng, H., and Y. Ben-Zion (2018a). Characteristics of airplanes and helicopters recorded by a dense seismic array near Anza California, *J. Geophys. Res.* **123,** no. 6, 4783–4797, doi: 10.1029/2017JB015240.

Meng, H., and Y. Ben-Zion (2018b). Detection of small earthquakes with dense array data: Example from the San Jacinto fault zone, southern California, *Geophys. J. Int.* **212,** no. 1, 442–457, doi: 10.1093/gji/ggx404.

Mordret, A., P. Roux, P. Boué, and Y. Ben-Zion (2018). Shallow three-dimensional structure of the San Jacinto fault zone revealed from ambient noise imaging with a dense seismic array, *Geophys. J. Int.* **216,** no. 2, 896–905, doi: 10.1093/gji/ggy464.

Naderyan, V., C. J. Hickey, and R. Raspet (2016). Wind-induced ground motion, *J. Geophys. Res.* **121,** no. 2, 917–930, doi: 10.1002/2015JB012478.

Nakata, N., J. P. Chang, J. F. Lawrence, and P. Boué (2015). Body wave extraction and tomography at Long Beach, California, with ambient-noise interferometry, *J. Geophys. Res.* **120,** no. 2, 1159–1173, doi: 10.1002/2015JB011870.

Prieto, G. A., R. L. Parker, and F. L. Vernon (2009). A Fortran 90 library for multitaper spectrum analysis, *Comput. Geosci.* **35,** no. 8, 1701–1710, doi: 10.1016/j.cageo.2008.06.007.

Ringler, A. T., R. E. Anthony, M. S. Karplus, A. A. Holland, and D. C. Wilson (2018). Laboratory tests of three Z-land fairfield nodal 5-Hz, three-component sensors, *Seismol. Res. Lett.* **89,** no. 5, 1601–1608, doi: 10.1785/0220170236.

Schmandt, B., and R. W. Clayton (2013). Analysis of teleseismic *P* waves with a 5200-station array in Long Beach, California: Evidence for an abrupt boundary to inner borderland rifting, *J. Geophys. Res.* **118,** no. 10, 5320–5338, doi: 10.1002/jgrb.50370.

Thomson, D. J. (1982). Spectrum estimation and harmonic analysis, *Proc. IEEE* **70,** no. 9, 1055–1096, doi: 10.1109/PROC.1982.12433.

Ward, K. M., and F. C. Lin (2017). On the viability of using autonomous three-component nodal geophones to calculate teleseismic *Ps* receiver functions with an application to Old Faithful, Yellowstone, *Seismol. Res. Lett.* **88,** no. 5, 1268–1278, doi: 10.1785/0220170051.

Wu, C., Z. Peng, and Y. Ben-Zion (2010). Refined thresholds for non-linear ground motion and temporal changes of site response associated with medium-size earthquakes, *Geophys. J. Int.* **182,** no. 3, 1567–1576, doi: 10.1111/j.1365-246X.2010.04704.x.

Wu, S.-M., K. M. Ward, J. Farrell, F.-C. Lin, M. Karplus, and R. B. Smith (2017). Anatomy of Old Faithful from subsurface seismic imaging of the Yellowstone Upper Geyser basin, *Geophys. Res. Lett.* **44,** no. 20, 10,240–10,247, doi: 10.1002/2017GL075255.

Christopher W. Johnson
Frank Vernon
UCSD/SIO/IGPP
9500 Gilman Drive, MC 0225
La Jolla, California 92093-0225 U.S.A.
cwj004@ucsd.edu

Nori Nakata
School of Geology and Geophysics
University of Oklahoma
100 East Boyd Street, RM 710
Norman, Oklahoma 73019 U.S.A.

Yehuda Ben-Zion
Department of Earth Sciences
University of Southern California
Zumberge Hall, Room 109
Los Angeles, California 90089-0740 U.S.A.

Published Online 24 April 2019

Downloaded from https://pubs.geoscienceworld.org/ssa/srl/article-pdf/90/4/1612/4790836/srl-2018383.1.pdf
by University of Southern California user